JLR RESEARCH ARTICLE

Bioavailability and spatial distribution of fatty acids in the rat retina after dietary omega-3 supplementation

Elisa Vidal[1,2], Bokkyoo Jun[3], William C. Gordon[3], Marie-Annick Maire[1], Lucy Martine[1], Stéphane Grégoire[1], Spiro Khoury[4], Stephanie Cabaret[4], Olivier Berdeaux[4], Niyazi Acar[1], Lionel Bretillon[1,*], and Nicolas G. Bazan[3]

[1]Eye and Nutrition Research Group, Centre des Sciences du Goût et de l'Alimentation, AgroSup Dijon, INRAE, CNRS, Université Bourgogne Franche-Comté, Dijon, France, [2]Horus Pharma Laboratories, Saint Laurent du Var, France, [3]Neuroscience Center of Excellence, School of Medicine, Louisiana State University Health New Orleans, New Orleans, LA, USA, and [4]Chemosens Group, Centre des Sciences du Goût et de l'Alimentation, AgroSup Dijon, CNRS, INRAE, Université Bourgogne Franche-Comté, Dijon, France

Abstract **Spatial changes of FAs in the retina in response to different dietary n-3 formulations have never been explored, although a diet rich in EPA and DHA is recommended to protect the retina against the effects of aging. In this study, Wistar rats were fed for 8 weeks with balanced diet including either EPA-containing phospholipids (PLs), EPA-containing TGs, DHA-containing PLs, or DHA-containing TGs. Qualitative changes in FA composition of plasma, erythrocytes, and retina were evaluated by gas chromatography-flame ionization detector. Following the different dietary intakes, changes to the quantity and spatial organization of PC and PE species in retina were determined by LC coupled to MS/MS and MALDI coupled to MS imaging. The omega-3 content in the lipids of plasma and erythrocytes suggests that PLs as well as TGs are good omega-3 carriers for retina. However, a significant increase in DHA content in retina was observed, especially molecular species as di-DHA-containing PC and PE, as well as an increase in very long chain PUFAs (more than 28 carbons) following PL-EPA and TG-DHA diets only. All supplemented diets triggered spatial organization changes of DHA in the photoreceptor layer around the optic nerve. Taken together, these findings suggest that dietary omega-3 supplementation can modify the content of FAs in the rat retina.**

Supplementary key words diet and dietary lipids • docosahexaenoic acid • eicosapentaenoic acid • lipid biochemistry • lipid spatial organization • omega-3 fatty acids • phosphatidylcholine • phospholipids • triglycerides • very long chain polyunsaturated fatty acids

Age-related macular degeneration (AMD) is the most common cause of blindness after the age of 55 years in Western populations and the third most common cause of severe visual impairment worldwide (1, 2). High dietary intake of omega-3 (n-3) long chain (LC)-PUFAs (C18–22) is associated with a lower risk of developing AMD (3). In the Blue Mountains Eye Study population, participants in the highest quantile of n-3 polyunsaturated fat intake had a lower risk of incident early age-related maculopathy compared with those in the lowest quantile (odds ratio: 0.41). Consumption of fish at least three times a week was associated with a reduced incidence of late age-related maculopathy (odds ratio: 0.25). Moreover, a higher intake of EPA (20:5, n-3) and DHA (22:6, n-3) was protective against the progression of AMD (4). A study revealed that during early and intermediate AMD, the DHA content of the retina was reduced (5). DHA is the major retinal n-3 long chain PUFA (LC-PUFA). In the human retina, its concentration is greater than 15% of the total FAs (6, 7). This FA plays a key role in vision and constitutes up to 50% of the fatty acids in the discs of photoreceptor outer segments, where it provides fluidity by favoring conformational changes of rhodopsin during phototransduction (8–12). Photoreceptor cells express the elongase enzyme, elongation of very long chain FAs (ELOVL)4, which catalyzes the biosynthesis of very long chain PUFAs (≥C28) including n-3 (VLC-PUFAs, n-3) from 26:6 FAs derived from DHA or EPA; EPA is the preferred substrate. Even though the levels of EPA are quite low in the retina compared with DHA, retroconversion of DHA to EPA in peroxisomes takes place, and it is possible that EPA produced by this reaction will generate the 26:6 substrate for ELOVL4 (13, 14). LC-PUFAs and VLC-PUFAs are able to produce lipid mediators named resolvins (15), protectins (16) from LC-PUFAs, or elovanoids from VLC-PUFAs (17) that show protective effects against inflammation and oxidative stress (18). In general, despite the endogenous capacity of human cells to synthesize EPA and DHA from their parent FA α-linolenic acid (ALA, 18:3, n-3), the extent to which it is converted to EPA and DHA is very weak, i.e., around 8% into EPA and 1% into DHA (19–22). Some Western countries have raised dietary recommendations for EPA and DHA intake to 500 mg/day to reduce the risk of developing AMD (23). EPA and DHA can either be provided by increasing consumption of seafood or via supplements. Many dietary supplements are composed of variable marine sources of n-3 LC-PUFA oils. In natural fish oil, EPA and DHA are mainly present as TGs and as phospholipids (PLs) in Antarctic krill oil. The

This article contains supplemental data.

*For correspondence: Lionel Bretillon, lionel.bretillon@inrae.fr.

DOI 10.1194/jlr.RA120001057

recommendations are not precise for supplementation chemical forms of EPA and DHA and often assume that different chemical forms have similar bioavailability. Bioavailability determines the extent to which an active substance is absorbed and transported through the systemic circulation. A greater bioavailability does not mean a greater distribution to the biological site, such as the retina. A greater distribution would be represented by a greater incorporation of EPA and DHA in the retina and would result in a greater functional benefit for the target.

The bioavailability of PUFAs depends on numerous factors including a matrix effect, i.e., whether the composition of food in macronutrients modifies the bioavailability of FAs (24). Among the factors affecting n-3 LC-PUFA incorporation is the dietary intake of linoleic acid (LA; 18:2, n-6) from the n-6 series because the incorporation of n-3 LC-PUFA is inversely associated with the intake of LA, particularly in the retina (25). Also, note that the protective effect of n-3 LC-PUFA intake against AMD was found primarily in patients with low dietary intake of LA (26). DHA bioavailability also depends on the chemical form of intake: free FAs, esters, TGs, or PLs (27). Moreover, the efficacy of EPA compared with DHA intake to increase the incorporation of DHA in the retina has not been studied. The present study aims to define the efficacy of different dietary formulations of TGs and/or PLs with EPA and DHA for their incorporation in plasma, erythrocytes, retinal pigment epithelial (RPE) cells, and retina in the rat. Our aim was to determine, using MALDI-imaging MS (MALDI-IMS), whether dietary supplementation with omega-3 FAs altered the cellular spatial distribution of FAs in the rat retina between photoreceptors and RPE cells.

MATERIALS AND METHODS

Standards and chemicals

Chloroform ($CHCl_3$) and methanol (CH_3OH) were purchased from Carlo Erba Reactifs SDS (Peypin, France). Ammonium acetate, acetonitrile (ACN), CH_3OH, and water of LC-MS grade were obtained from Fisher Scientific (Illkirch, France). Commercially available PL and TG standards were obtained from Avanti Polar Lipids Inc. (Alabaster, AL) and Matreya LLC (State College, PA). Other chemical reagents were purchased from Sigma-Aldrich (Saint Quentin Fallavier, France).

Experimental diets

Commercial high-oleic sunflower oil, sunflower oil, palm oil, rapeseed oil, linseed oil, fish oil (Polaris, Quimper, France), herring roe oil (Novastell, Etrépagny, France), krill oil (AkerBiomarine), and egg powder (Novastell, Etrépagny, France) were mixed in various proportions to prepare the five following blends: EPA-rich PLs (PL-EPA), DHA-rich PLs (PL-DHA), EPA-rich TGs (TG-EPA), DHA-rich TGs (TG-DHA), and no DHA and EPA (Control). The lipid blends were used to prepare rodent diets (SAFE diets, Augy, France). The five experimental diets had the same composition: casein 18%, corn starch 38.25%, dextrose 18%, sucrose 6%, oil 10%, cellulose 5%, minerals + vitamins 4.5%, and bitartrate choline 0.25%. As reported in **Table 1**, the four n-3 rich diets contained 7% of EPA + DHA, whereas the control diet contained no EPA and DHA. The five diets were designed to contain a ratio between 4 and 5 of LA to ALA. The distribution of lipid classes (**Table 2**) was determined using a combination of thin-layer chromatography on silica gel-coated quartz rods and flame ionization detection (Iatroscan system, Iatron, Tokyo, Japan) according to Ackman's technique (28) and as published by our group (7).

Animals

The ethics committee of our institution (Comité d'Ethique de l'Expérimentation Animale 105, Dijon, France) approved all interventions and animal care procedures. Male Wistar rats (4 weeks of age, n = 55) were purchased from Janvier Labs (Le Genest-Saint-Isle, France). They were housed in a controlled environment at 23 ± 1°C, 55–60% humidity, under a 12 h light/12 h dark cycle, 780 lux in light phase, and had free access to food and tap water. The rats were acclimatized for 2 weeks and fed on a standard rodent chow (Rat No.1 Maintenance, Special Diets Services, UK) before they were fed on a chow described in the "Experimental diets" section for 8 weeks. The rats were then randomly divided into five groups of 11 rats each (four cages of two rats and one cage of three rats per group). The rats' food and water were weighed once a week.

Collection of samples

At the end of the 8 week feeding period, animals were fasted overnight; they were weighed and then euthanized by an intraperitoneal injection of pentobarbital (Ceva, Santé animale, Libourne, France) at a lethal dose (150 mg/kg body weight) and exsanguinated by intracardiac puncture. Plasma was separated from red blood cells (RBCs) by centrifugation (1,811 *g* during 20 min, 4°C), and both were kept at −80°C until further FA analyses. Retinas were collected from eight rats per group and frozen in liquid nitrogen and stored at −80°C for FA analyses. Rat eyeballs from three rats per group were fast frozen in liquid nitrogen and stored at −80°C for MALDI-IMS analyses (see below) and RPE/choroid layer analyses.

Lipid extraction and distribution

Total lipids were extracted from the retinas and experimental diets following the Folch method (29), whereas they were isolated from erythrocytes and plasma according to the method of Moilanen and Nikkari (30). Total lipids from each diet were submitted to a thin-layer chromatography separation on precoated silica gel plates (Merck, Darmstadt, Germany) using a solvent mixture of hexane/diethyl ether/acetic acid (80:20:1, v/v/v). The silica gel plates were visualized under UV light (360 nm) after spraying with 2′,7′-dichlorofluorescein. The spots corresponding to PLs and TGs were scraped off the plate, and the samples were transesterified following the FA analysis procedure (see below).

Analysis of FAs in plasma, RBC, and retina samples by gas chromatography

FAs were converted into methyl esters according to Morrison and Smith (31) and analyzed as previously described (7). FA methyl esters were extracted with hexane and analyzed by gas chromatography on a Hewlett Packard Model 5890 gas chromatograph (Palo Alto, CA) using a CPSIL-88 column (100 m × 0.25 mm i.d., film thickness 0.20 μm; Varian, Les Ulis, France) equipped with a flame ionization detector. Hydrogen was used as the carrier gas (inlet pressure, 210 kPa). The injection volume was 1 μl. The oven temperature was held at 60°C for 5 min, increased to 165°C at 15°C/min and held for 1 min, and then to 225°C at 2°C/min and finally held at 225°C for 17 min. The injector and the detector were maintained at 250°C. The data were processed

TABLE 1. FA composition of the diets

Percent of Total FAs	Control	PL EPA	PL DHA	TG EPA	TG DHA
Saturated fatty acids	26.81	27.53	29.97	27.51	27.13
12:0	0.13	0.14	0.04	0.09	0.11
14:0	0.62	1.86	0.82	0.60	0.57
15:0	0.05	0.11	0.16	0.06	0.04
16:0	21.35	21.16	20.64	22.00	21.85
17:0	0.08	0.09	0.22	0.07	0.07
18:0	3.82	3.44	7.47	3.84	3.72
20:0	0.32	0.27	0.15	0.33	0.30
22:0	0.31	0.24	0.30	0.29	0.30
24:0	0.13	0.22	0.14	0.20	0.18
dma16:0	—	—	0.13	—	—
dma18:0	—	—	0.15	—	—
MUFAs	60.01	49.92	46.79	49.60	49.70
16:1n-9	0.04	0.05	0.08	—	—
16:1n-7	0.18	1.20	1.01	0.16	0.18
18:1n-9	56.49	44.68	42.54	46.65	47.03
18:1n-7	1.88	3.02	2.31	1.69	1.67
18:1 t	1.20	0.51	0.65	0.60	0.42
20:1n-9	0.19	0.26	0.15	0.43	0.30
22:1n-9	—	0.14	0.05	—	—
24:1n-9	0.01	0.07	—	0.07	0.10
dma18:1n-9	—	—	0.12	—	—
PUFAs	13.20	22.54	22.87	22.92	23.16
18:2n-6 (LA)	10.67	12.61	10.96	11.74	12.37
18:2 tc	0.15	0.14	0.08	0.15	0.15
18:2 ct	0.14	0.12	0.06	0.13	0.13
18:3n-6	—	—	0.07	0.10	0.10
20:2n-6	0.05	0.05	0.09	0.07	0.07
20:3n-6	—	—	0.10	0.06	0.03
20:4n-6 (AA)	—	0.15	1.03	0.35	0.21
22:4n-6	—	—	0.06	—	0.04
22:5n-6 (DPA n-6)	—	—	0.13	0.14	0.25
18:3n-3 (ALA)	2.19	2.60	2.36	2.46	2.58
20:5n-3 (EPA)	—	4.48	2.18	5.44	2.70
22:5n-3 (DPA n-3)	—	0.11	0.20	0.14	0.26
22:6n-3 (DHA)	—	2.28	5.55	2.14	4.27
LA/ALA ratio	4.87	4.85	4.64	4.77	4.79

using the EZChrom Elite software (Agilent Technologies, Massy, France). FA results were expressed in percent of all identified FAs.

Chromatographic separation of PLs

PL classes were separated by LC under hydrophilic interaction LC (HILIC) conditions using an Accucore™ HILIC LC column (150 × 2.1 mm, 2.6 μm; Thermo). HPLC separation was performed using an UltiMate™ 3000 LC pump equipped with a dual-gradient pump and an UltiMate™ 3000 autosampler from Thermo Scientific. The mobile phase consisted of (A) ACN/water (95:5, v/v) containing 5 mM ammonium acetate and (B) ACN/water (50:50, v/v) containing 10 mM ammonium acetate. The solvent-gradient system of the analytical pump was as follows: 0 min 100% A, 1 min 95% A, 20 min 80% A, 23 min 65% A, 24 min 100% A, and 24–39 min 100% A. The flow rate was 800 $\mu l \cdot min^{-1}$. The flow from LC was split using an analytical fixed flow splitter (split ratio = 1:1, postcolumn) from Analytical Scientific Instruments (El Sobrante, CA). The injection volume was 10 μl. The column was maintained at 40°C. The LC system was controlled by Standard Instrument Integration (SII) software based on Dionex Chromeleon™ 7.

Characterization of PL species (Orbitrap FUSION™)

Samples of the same groups were pooled to characterize PL species. The Orbitrap Fusion™ Tribrid mass spectrometer (Thermo Scientific) was used for high-resolution analyses. This instrument was equipped with an EASY-MAX NG™ ion source [heated ESI (H-ESI)] and was controlled by Xcalibur™ 4.1 software. Positive and negative ions were monitored alternatively by switching polarity with a spray voltage set to 3,500 V in positive and negative ion modes. The Orbitrap mass analyzer was employed to obtain all mass spectra in full scan mode with the normal mass

TABLE 2. EPA and DHA containing TGs and PLs in diets

Lipid Classes Content (%)	Control	PL EPA	PL DHA	TG EPA	TG DHA
TG	90.5	73.3	48.4	89.6	87.7
DHA	—	0	0	0.6	1.6
EPA	—	0.1	0	2.3	1
PL	0	21.4	49.7	0	0
DHA	—	11.8	9.8	—	—
EPA	—	23.3	3.9	—	—
Cholesterol	0	0.5	0.4	0	0
DAG	6.8	4.8	1.5	6.2	5.8
MAG	2.7	0	0	4.2	6.5

range and a target resolution of 240,000 (FWHM at *m/z* 200). A dynamic exclusion filter was applied with an exclusion duration of 15 s and a mass tolerance of 5 ppm. For MS/MS analyses, data-dependent mode was used for the characterization of PL species. Precursor isolation was performed in the quadrupole analyzer with an isolation width of *m/z* 1.6. Higher-energy collisional dissociation was employed for the fragmentation of PLs with an optimized stepped collision energy of 30% (±5%). The linear ion trap was used to acquire spectra for fragment ions in data-dependent mode. The automatic gain control target was set to 2×10^4 with a maximum injection time of 50 ms. The identification of PL species was performed with the help of LipidSearch™ software based on the data of high accuracy and on MS/MS experiments.

Quantification of PL species

The phosphorus content of the total lipid extract was determined according to the method developed by Bartlett and Lewis (32). The PL samples were then diluted to the appropriate concentration of 25 $\mu g \cdot ml^{-1}$ of PLs in $CHCl_3/CH_3OH$ (1:1, v/v). Internal PL standards composed of 1,2-dimyristoyl-*sn*-glycerol-3-PE (PE 14:0/14:0 at 0.2 $\mu g \cdot ml^{-1}$), 1,2-dimyristoyl-*sn*-glycerol-3-PC (PC 14:0/14:0 at 0.4 $\mu g \cdot ml^{-1}$) and 1,2-dilignoceroyl-*sn*-glycero-3-phosphocholine (PC 24:0/24:0 at 0.4 $\mu g \cdot ml^{-1}$) were added to the samples for quantification purposes.

The HPLC system under the previously described HILIC conditions was coupled to a triple quadrupole mass spectrometer (QqQ, Thermo Finnigan TSQ Quantum) equipped with a standard electrospray ionization source. The electrospray ionization spray voltages were −3 kV and 4.5 kV in the negative and positive ion modes, respectively; the vaporizer temperature was 150°C; the sheath gas N_2 pressure was 45 au; the auxiliary gas pressure was 45 au; the ion sweep gas pressure was 5; the ion transfer capillary temperature was 300°C; the skimmer offset was 5 V; and the multiplier gain was 300,000.

PL species were analyzed in specific acquisition modes using this QqQ instrument. PC species were quantified in positive ion mode by precursor ion scanning of *m/z* 184 amu, which corresponds to the choline head group. PE species lose their ethanolaminephosphate head group as a neutral fragment of 141 Da. Therefore, neutral loss scanning of 141 Da in positive ion mode was used for the selective detection and quantification of PE. The data were processed using Xcalibur software. In addition, the extraction of the selected masses was carried out using the Igor Pro software (Igor Pro 7.0, WaveMetrics Inc., Portland, OR), and corrections were applied to the data for isotopic overlap.

More details about the electrospray source parameters and mass spectrometer methods are available in (33).

Preparation of retinas for MALDI-IMS

As recently published by Kautzmann et al. (34), the eyeballs were embedded in 20% gelatin (DIFCO, Sparks, MD) before they were cryosectioned using a cryostat (Thermo Fisher/Shandon, Pittsburg, PA) to obtain 15 μm-thick transverse sections showing all layers of the retina, choroid, optic nerve, and sclera. Sections were attached to glass coverslips and stored in a desiccator until needed for MALDI imaging. Alternate sections were kept on slides and stained with H&E for orientation purposes. For this study, in total, more than 10 individual sections per group were analyzed in positive ion mode by MALDI-IMS.

Matrix application for MALDI-IMS

The glass coverslips containing the retina sections were placed on the MALDI plate inserts using thermally conductive dual tape, and the 2,5-dihydroxybenzoic acid (DHB; Fisher Scientific, Pittsburg, PA) matrix was deposited by sublimation (35). The conditions during sublimation of the DHB matrix were a pressure of 0.05 Torr, condenser temperature of 15°C, and 300 mg DHB in the sublimator. The heat was applied progressively until 130°C in 11 min.

MALDI-MS imaging analysis

A quadrupole-TOF tandem mass spectrometer with an orthogonal MALDI source (MALDI Synapt G2-Si; Waters; Mildford, MA) was used to acquire mass spectral data from which images were constructed. MALDI mass spectra were obtained using a solid state laser (355 nm) at an energy of 7.4 J and a pulse rate of 2,000 Hz for positive ion MALDI imaging. The energy and pulse rate of the laser were selected to maximize the lipid signal from the tissue slice. The positive ion MALDI imaging experiments had an accumulation time of 243 ms per image spot. The MALDI plate was moved at a rate of 12.75 $mm \cdot min^{-1}$, and after each horizontal line was completed, the plate was moved vertically 30 μm. The lateral resolution of this MALDI-IMS technique has been estimated to be approximately 30 μm. The mass spectrometric data were processed using a specialized script for Analyst software (Waters) at a mass resolution of 0.1 amu. The lipids observed in positive ion mode (PC, SM, and TG) were identified to the lipid species level by ion mobility separation with helium gas (DriftScope, Waters) used in conjunction with ToF. Data were processed with HDImaging, and MALDI images were visualized using Biomap software (Novartis), with the same intensity between samples per ion.

Statistical analysis

Data were analyzed using the Kruskal Wallis test, followed by Dunn's post hoc test when appropriate. The level of significance was set at $P \leqslant 0.05$. All results were analyzed using GraphPad Prism version 7.00 for Windows (GraphPad Software, San Diego, CA). Data are presented as mean ± SD.

RESULTS

General observations

No abnormalities were noted in the general appearance of the rats; body weight and food intake did not differ over the 8 weeks of the experimental period in any of the groups (supplemental Table S1).

n-3 PUFA supplementation increases EPA and DHA in plasma

The plasma DHA level was significantly higher in both DHA-supplemented groups compared with animals from the control group ($P < 0.001$) with no difference between PL-DHA and TG-DHA groups ($P > 0.05$). There was no statistically significant difference in plasma DHA levels between EPA-supplemented groups and controls. Plasma levels of EPA and docosapentaenoic acid (DPA) n-3 were significantly increased by PL-EPA and TG-EPA diets compared with the control-diet: ×20 for EPA, ×3 for DPA n-3 ($P < 0.001$). Among n-6 FAs, plasma LA (18:2 n-6) was significantly higher for all formulations with the exception of the PL-DHA diet compared with the control diet group (+34% in PL-EPA vs. control, $P < 0.001$; +24% in TG-EPA vs. control, $P < 0.05$; +34% in TG-DHA vs. control, $P < 0.001$). The level of AA (20:4 n-6) in plasma was reduced by half in the

PL-EPA group ($P < 0.001$) and by 40% in the TG-DHA group ($P < 0.01$) compared with control group. There was no difference in plasma FA composition between the PL-EPA and TG-EPA groups on the one hand, and between PL-DHA and TG-DHA diet groups on the other hand (**Fig. 1A**, supplemental Table S2).

n-3 PUFA supplementation increases n-3 index

In RBCs, the DHA level was increased by a factor of two in both PL-DHA and TG-DHA groups ($P < 0.001$) and to a lesser extent in the PL-EPA diet group (+73%, $P < 0.05$) compared with the control diet group. The DPA n-3 (22:5, n-3) level was significantly increased in erythrocytes by all the four formulations compared with control diet ($P < 0.001$, +61–180%). Meanwhile, the EPA level in erythrocytes was tremendously increased in the PL-EPA and TG-EPA groups (×16–18, $P < 0.001$). The n-3 index was tremendously increased in all groups (not statistically significant for the PL-DHA group) compared with the control diet group. Among n-6 FAs, the LA (18:2, n-6) level was higher in the PL-EPA and TG-DHA groups compared with the control diet group ($P < 0.001$). The AA (20:4, n-6) level was significantly lower in all groups ($P < 0.01$), except in PL-DHA, compared with control-diet group. There was no difference for any FA between the PL-EPA and TG-EPA groups on the one hand and between the PL-DHA and TG-DHA groups on the other hand (Fig. 1B, supplemental Table S3).

PL-EPA and TG-DHA diets have similarities in changing the n-3 FA profile in the retina

The heatmap in **Fig. 2** revealed two main clusters in retina, with red and green indicating increased and decreased relative abundance in a same row, respectively. In this analysis, PL-EPA and TG-DHA have a similar profile with a decrease in the abundance of saturated, monounsaturated, and n-6 FAs, and an increase in the abundance of n-3 PUFAs. As shown in **Table 3**, with the exception of the PL-DHA group, which showed a nonstatistically significant increase compared with the control diet group, the EPA level in the retina was higher in all supplemented groups versus control: ×6 in PL-EPA ($P < 0.001$), ×5 in TG-EPA ($P < 0.01$), and ×4.7 in TG-DHA ($P < 0.05$). The DHA level was significantly increased in the retina by +23% in PL-EPA ($P < 0.001$), +19% in PL-DHA ($P < 0.05$), and +24% in TG-DHA ($P < 0.001$), compared with control diet. The 8% increase of retinal DHA in animals fed with TG-EPA remained statistically not significant compared with the control ($P > 0.05$). The increase of DHA and total n-3 PUFAs in retina is independent of PL and TG content of diets (no difference between PL-EPA and TG-EPA and PL-DHA and TG-DHA). The DPA n-3 (22:5 n-3) level was increased by 2.6-fold in EPA-rich diet groups compared with control ($P < 0.001$). Among n-6 FAs, AA was less abundant in the retina of animals fed with TG diets ($P < 0.01$). DPA n-6 (22:5 n-6) was tremendously reduced by a factor of three to six in the retina of the animals fed with the four supplemented diets (not statistically significant for TG-DHA).

PL-EPA and TG-DHA diets increase DHA in retinal PC and PE as well as VLC-PUFAs

Retinal PCs contain a significant amount of di-saturated FAs (15% of PC32:0, 16:0/16:0), saturated/monounsaturated FAs (17% of PC34:1, 16:0/18:1), and saturated/polyunsaturated FAs (20%, PC40:6, 18:0/22:6). PC is the only class that contained detectable levels of VLC-PUFAs with more than 24 carbons in length. Our results showed that the sum of VLC-PUFAs in the retina was significantly higher in PL-EPA and TG-DHA diet groups compared with the control group. This increase concerned particularly PC54:12 (32:6/22:6) and PC54:11 (32:5/22:6). There was a statistically significant increase in PC44:12 (22:6/22:6) in the retina of PL-EPA, PL-DHA, and TG-DHA diet groups, and a significant increase of PC40:6 (18:0/22:6) in the TG-DHA diet group compared with the control (**Fig. 3A**, supplemental Table S4). PC54:11 and 54:12, containing 32 and 34 carbon VLC-PUFAs, were also increased compared with controls. Retinal PE showed a large proportion of PL rich in saturated/polyunsaturated FAs: 50% of PE40:6 (18:0/22:6), 10% of PE38:6 (16:0/22:6), and 15% of PE44:12 (22:6/22:6). Our results revealed that feeding rats with PL-EPA and TG-DHA triggered a significant increase in PE44:12 (22:6/22:6) and decrease in PE42:10 (20:4/22:6) (Fig. 3B, supplemental Table S5). Within the RPE/choroid, our preliminary results indicate that these PCs also supplied similar or significantly less EPA or DHA, with the exception of PC38:6 (16:0/22:6). This was increased with all diets by about 90% (**Fig. 4**). Importantly, the PL-DHA diet maintained concentrations similar to that supplied by the control diet.

DHA uptake takes place in the photoreceptor layer around the optic nerve

Figure 5 illustrates a typical eye section stained with H&E. It shows connective tissue, sclera, optic nerve, RPE, choroid, and retinal layers. The spatial localization of the lipid molecular species was determined using MALDI-IMS in coronal sections of the ocular globes. Ion mobility separation

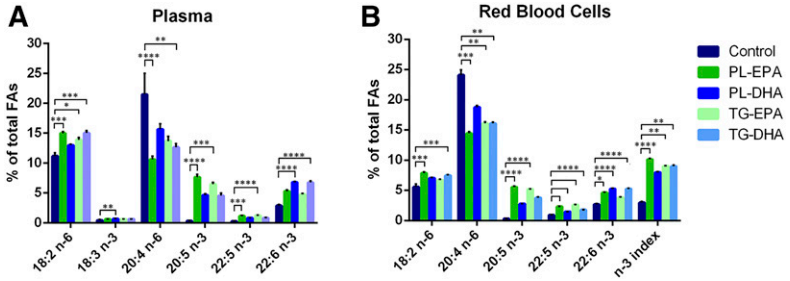

Fig. 1. The omega-3 (n-3) index is increased in all supplemented groups. Relative percent of relevant FAs from FA in plasma (A) and erythrocytes (B) performed by gas chromatography followed by flame ionization detection. Bars represent the mean + SD. *P* values were determined by Kruskal Wallis test. *$P < 0.05$, **$P < 0.01$, ***$P < 0.001$, ****$P < 0.0001$.

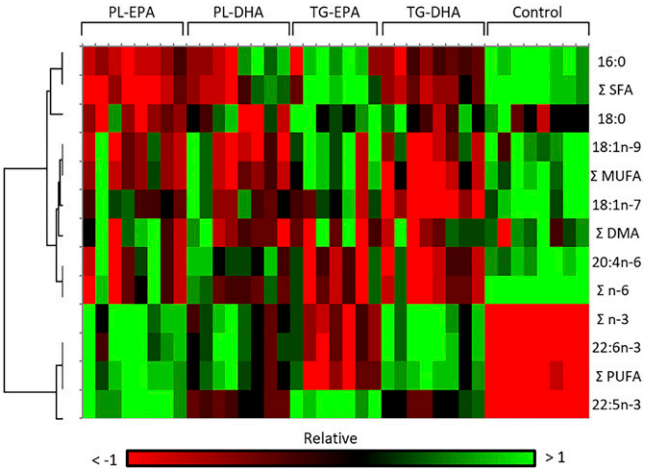

Fig. 2. Heat map showing the hierarchical clustering of significant differences occurring in FA species (relative to total FAs, defined as 100%) in PL-EPA, PL-DHA, TG-EPA, and TG-DHA retinas compared with the control group. PL-EPA and TG-DHA groups present similar profiles compared with other groups. The heat map was created with XLSTAT (by Addinsoft). Filtering was performed by interquartile range under the threshold of 0.25.

coupled with ToF was used to determine the composition in lipid/PC molecular species (supplemental Table S6). The positive ion mass spectra were obtained in the mass range of *m/z* 450–1,100 amu. The spectra illustrated the distribution of the lipid molecular species within the different regions of the eye tissue: inner retina, outer retina, and orbital fat. Positive ion data obtained for the MALDI-IMS experiments revealed the distribution of PC and TG lipids in the ocular section.

In the region of interest of the inner retina, the positive ion MALDI mass spectrum indicated a peculiar molecular species profile with the most intense ion at *m/z* 782.6 amu corresponding to PC34:1 (16:0/18:1) (**Fig. 6A**, D). The positive ion MALDI image at *m/z* 782.6 amu suggested that this ion was present within the inner retina composed of ganglion cells, nerve fiber layer, optic nerve, and a thin region beneath the outer retina (Fig. 6G) previously identified as the blood vessels in the choriocapillaris (36). The positive ion MALDI mass spectrum revealed the presence of less intense lipids in this region at *m/z* 756.6 amu that were not unique to this location. This molecular species at *m/z* 756.6 amu corresponds to a PC32:0 (most likely 16:0/16:0), which was intense in all retinal layers, including the outer retina, as shown by MALDI-IMS.

The MALDI mass spectrum of the outer retina, including the outer segments of the photoreceptor cells, identified the most intense ion at *m/z* 756.6 amu (PC32:0, 16:0/16:0). As presented above, this ion was present in the entire retina and was not specific to the outer retina (Fig. 6B, E). The spectrum of the outer retina also revealed two molecular species at *m/z* 856.6 and 900.6 amu, which may correspond to sodiated PC40:6 (18:0/22:6) and PC44:12 (22:6/22:6), respectively. The positive ion MALDI image at *m/z* 856.6 and 900.6 amu indicated that these lipids were exclusively localized in the photoreceptor layer (Fig. 6H).

The area corresponding to orbital fat revealed a MALDI mass spectrum with the most intense ion at *m/z* 881.8 amu (Fig. 6C, F). The positive ion MALDI image at *m/z* 881.8 amu suggested that the ion was present within the tissue surrounding the optic nerve and likely corresponds to the orbital fat (Fig. 6I). The black areas within this structure could correspond to cross-sectioned blood vessels. The molecular species *m/z* 881.8 amu has been previously identified as TG$[M+Na]^+$ denoted as TG52:2 (16:0/18:1/18:1 or 16:0/18:0/18:2). Additionally, the nonidentified molecular species at *m/z* 853.8 amu was found with similar regional distribution to *m/z* 881.8 amu.

The merged images of the ions at *m/z* 782.6 [PC34:1+Na], 856.6 [PC40:6+Na], and 881.8 amu [TG52:2+Na] illustrate the spatial organization of these molecular lipids within the eye (Fig. 6J). The merged images of the ions at *m/z* 856.6 [PC40:6, 18:0/22:6+Na] (**Fig. 7A**) and 900.6 amu [PC44:12, 22:6/22:6+Na] (Fig. 7B) suggested that both species partially colocalized in the outer part of the photoreceptor layer. Meanwhile, the ion at *m/z* 856.6 amu [PC40:6+Na] extended more inward (Fig. 7C), meaning that each LC-PUFA-containing PC presents their own spatial distribution.

The retina is characterized by its content in VLC-PUFA-containing PC having 24 to 36 carbons and up to four double bonds in the mass range of *m/z* 900–1,100 amu. Within the photoreceptor layer, we identified in the positive ion MALDI spectrum molecular species at *m/z* 1,018.7, 1,040.7, and 1,068.7 amu with a lower signal than other species previously identified (**Fig. 8A**). These molecular species were previously identified as VLC-PUFAs-containing PC as [PC52:9, 30:3/22:6+Na], [PC54:12, 32:6/22:6+Na], and [PC56:12, 34:6/22:6+Na], respectively (36), and we have confirmed this using ion mobility.

The merge of MALDI images at both *m/z* 900.6 [PC44:12, 22:6/22:6+Na] (Fig. 8B) and 1018.7 amu [PC52:9, 30:3/22:6+Na] (Fig. 8C) showed that these two species did not completely colocalize, but both were located in the photoreceptor layer (merge with H&E image, data not shown). PC44:12 is localized in an inner part of the photoreceptor layer compared with the location of PC52:9 (Fig. 8D).

The aim of this study was to localize the changes in FA location within the retina, especially DHA, following 8 weeks of PUFA-rich diet. The MALDI image at *m/z* 900.6 amu (PC44:12+Na) indicated the presence of this species with varied abundance throughout the retina in all supplemented groups compared with control group (**Fig. 9**). The more abundant signal for *m/z* 900.6 amu in the retina was observed in the photoreceptor layer surrounding the optic nerve. The distribution of *m/z* 900.6 amu outside this area was similar between groups. Moreover, the ion *m/z* 881.8 amu, corresponding to (TG52:2+Na), was more abundant in the supplemented-diet group compared with the retina of control diet.

The merged images of the lipid molecular ions at *m/z* 782.6 (PC34:1+Na), 900.6 (PC44:12+Na), and 881.8 amu (TG52:2+Na) nicely mapped the spatial organization of the eye (Fig. 9).

TABLE 3. FA composition of total lipids from rat retina tissue following supplemented diets

Percent of Total FAs	Control	PL-EPA	PL-DHA	TG-EPA	TG-DHA
14:0	0.16 ± 0.03	0.07 ± 0.01[a]	0.10 ± 0.05	0.16 ± 0.05	0.07 ± 0.02[b,c]
15:0	0.08 ± 0.02	0.05 ± 0.01[a]	0.07 ± 0.02	0.08 ± 0.02	0.05 ± 0.01[b,c]
dma 16:0	0.88 ± 0.08	0.85 ± 0.08	0.86 ± 0.09	0.86 ± 0.1	0.83 ± 0.04
16:0	20.18 ± 0.58	16.47 ± 0.53[d]	17.78 ± 2.01[a]	18.65 ± 2.02	16.86 ± 0.86[a]
16:1n-9	0.21 ± 0.02	0.15 0.01[b]	0.17 ± 0.03	0.19 ± 0.03	0.15 ± 0.01[d]
16:1n-7	0.37 ± 0.06	0.30 ± 0.05	0.36 ± 0.07	0.40 ± 0.12	0.26 ± 0.02[b,e,f]
17:0	0.15 ± 0.01	0.14 ± 0.01	0.17 ± 0.02	0.15 ± 0.01	0.13 ± 0.01[a,g]
dma 18:0	2.75 ± 0.08	2.83 ± 0.12	2.72 ± 0.11	2.76 ± 0.14	2.83 ± 0.11
dma 18:1n-9	0.41 ± 0.04	0.37 ± 0.04	0.37 ± 0.03	0.38 ± 0.03	0.36 ± 0.02
dma 18:1n-7	0.21 ± 0.03	0.22 ± 0.05	0.21 ± 0.04	0.19 ± 0.03	0.17 ± 0.02[a,h]
18:0	25.35 ± 0.56	24.80 ± 0.45[c]	24.94 ± 0.91	26.06 ± 0.86	25.46 ± 0.65
18:1t	0.05 ± 0.01	0.04 ± 0.01	0.06 ± 0.01	0.05 ± 0.01	0.04 ± 0.0[b,c,i]
18:1n-9	9.16 ± 0.29	8.55 ± 0.46	8.48 ± 0.44[a]	9.05 ± 0.47	8.43 ± 0.35[a]
18:1n-7	2.48 ± 0.16	2.27 ± 0.18	2.23 ± 0.17	2.21 ± 0.15	1.90 ± 0.12[d,h]
18:2n-6	0.76 ± 0.11	0.87 ± 0.09	0.74 ± 0.1	0.92 ± 0.12	0.8 ± 0.06
20:0	0.11 ± 0.02	0.09 ± 0.02	0.09 ± 0.02	0.14 ± 0.02[e,h,j]	0.09 ± 0.01[a]
20:1n-9	0.17 ± 0.01	0.13 ± 0.0[a]	0.14 ± 0.02[a]	0.16 ± 0.03	0.17 ± 0.02
20:1n-7	0.04 ± 0.0	0.03 ± 0.01[f]	0.04 ± 0.02	0.06 ± 0.02	0.05 ± 0.02
20:2n-6	0.09 ± 0.01	0.09 ± 0.01	0.09 ± 0.01	0.09 ± 0.01	0.09 ± 0.01
20:3n-9	0.05 ± 0.01	0.05 ± 0.03	0.06 ± 0.04	0.08 ± 0.04	0.04 ± 0.01
20:3n-6	0.13 ± 0.01	0.17 ± 0.0[d,g]	0.13 ± 0.01	0.15 ± 0.02	0.15 ± 0.01
20:4n-6	8.72 ± 0.31	8.10 ± 0.49	8.33 ± 0.23	7.86 ± 0.52[b]	7.85 ± 0.31[b]
20:5n-3	0.07 ± 0.02	0.42 ± 0.05[d,i]	0.27 ± 0.04	0.35 ± 0.04[b]	0.33 ± 0.05[a]
24:0	0.04 ± 0.01	0.05 ± 0.02	0.06 ± 0.01	0.09 ± 0.02[b,k]	0.04 ± 0.01
22:4n-6	1.24 ± 0.06	0.91 ± 0.06[b]	1.01 ± 0.08	0.90 ± 0.08[d]	0.90 ± 0.05[d]
22:5n-6	0.59 ± 0.1	0.10 ± 0.01[d,l]	0.14 ± 0.01[a]	0.13 ± 0.02[b]	0.15 ± 0.02
22:5n-3	0.34 ± 0.03	0.89 ± 0.06[d,e]	0.62 ± 0.05	0.88 ± 0.04[d,e]	0.67 ± 0.07
22:6n-3	25.09 ± 0.5	30.87 ± 1.28[d]	29.77 ± 1.65[a]	27.02 ± 1.61	31.15 ± 1.18[c,d]
Total of n-3 PUFAs	25.51 ± 0.5	32.19 ± 1.32[d]	30.67 ± 1.64[a]	28.25 ± 1.58	32.15 ± 1.11[d]
Total n-6 PUFAs	11.55 ± 0.39	10.27 ± 0.63[a]	10.44 ± 0.35	10.05 ± 0.60[b]	9.95 ± 0.40[d]
Total PUFAs	37.12 ± 0.60	42.51 ± 0.90[d,f,l]	41.17 ± 1.53[a]	38.38 ± 1.72	42.15 ± 0.89[b]
Total SFAs	46.11 ± 0.61	41.71 ± 0.71[d,f]	43.21 ± 1.43[a]	45.33 ± 1.30	42.70 ± 0.58[a]
Total MUFAs	12.51 ± 0.44	11.50 ± 0.68	11.47 ± 0.62	12.11 ± 0.67	10.97 ± 0.45[d]
n-6/n-3 PUFAs	0.45 ± 0.01	0.32 ± 0.03[d]	0.34 ± 0.03	0.36 ± 0.03	0.31 ± 0.02[d]

Values are mean ± SD (n = 8 rats per group). Probabilities were determined by Kruskal Wallis test followed by the Dunn's post hoc test. DMA, dimethyl acetal; SFA, saturated FA.

[a] $P < 0.05$ when the supplemented groups were compared with the control group.
[b] $P < 0.01$ when the supplemented groups were compared with the control group.
[c] $P < 0.05$ when the supplemented groups were compared with the TG-EPA group.
[d] $P < 0.001$ when the supplemented groups were compared with the control group.
[e] $P < 0.05$ when the supplemented groups were compared with the PL-DHA group.
[f] $P < 0.01$ when the supplemented groups were compared with the TG-EPA group.
[g] $P < 0.001$ when the supplemented groups were compared with the PL-DHA group.
[h] $P < 0.05$ when the supplemented groups were compared with the PL-EPA group.
[i] $P < 0.01$ when the supplemented groups were compared with the PL-DHA group.
[j] $P < 0.001$ when the supplemented groups were compared with the TG-DHA group.
[k] $P < 0.01$ when the supplemented groups were compared with the TG-DHA group.
[l] $P < 0.05$ when the supplemented groups were compared with the TG-DHA group.

DISCUSSION

Rodents are devoid of macula and cannot therefore be used to recapitulate the process of AMD. But they have been of interest as preclinical models of lipid absorption (37–40) or retinal diseases (41, 42) because they share similar mechanical features with humans. The consumption of foods rich in n-3 LC-PUFAs was associated with a lower risk of developing vascular and degenerative retinal diseases in humans (26, 43, 44). Nevertheless, data in humans suggested that the extent to which dietary LC-PUFAs contribute to their retinal levels remains controversial and

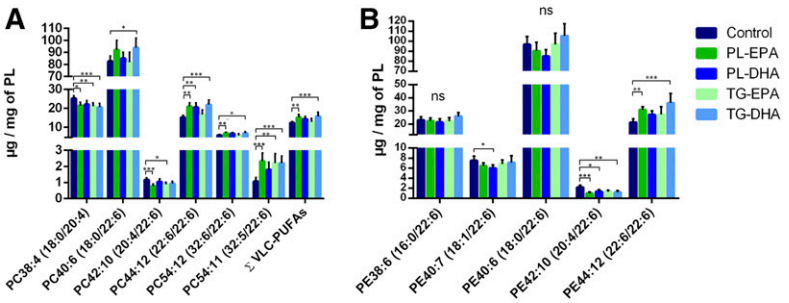

Fig. 3. In retina, PL-EPA and TG-DHA groups showed an increase in most DHA-containing PC and PE and VLC-PUFAs. Quantitative amounts of relevant species contained within PC (A) and PE (B) in the retina. Bars represent the mean + SD. *P* values were determined by Kruskal Wallis test, compared with the control group. $*P < 0.05$, $**P < 0.01$, $***P < 0.001$.

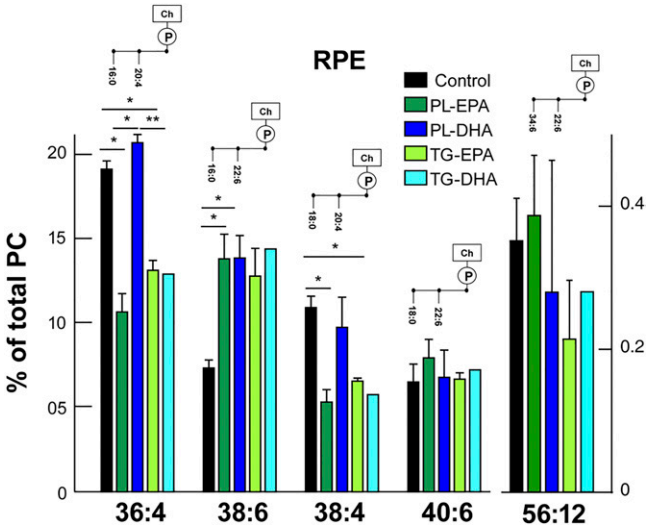

Fig. 4. In RPE, PC36:4 and PC38:4 show significant decreases in PL-EPA and TG-EPA, but not in PL-DHA. PC38:6, however, shows a significant increase in PL-EPA and PL-DHA groups compared with the control group. Bars represent the mean + SD, n = 3. *P* values were determined by Kruskal Wallis test, compared with the control group. $*P < 0.05$.

partial (7, 45, 46). The bioavailability of n-3 FAs from the diet depends on their chemical form (24). Only a few studies suggested that FAs provided as PLs are better absorbed than as TGs (47–49). Yet, these studies did not match similar doses as either PL and TG or as EPA and DHA (27), except one that revealed no difference in plasma n-3 provided either as TG or PL forms (50). Moreover, studying plasma leads to a high degree of uncertainty about the extent of incorporation of n-3 into the retina.

The goal of this study was to provide a novel molecular characterization of the retina of rats fed with different n-3-rich diets. Moreover, we wanted to provide qualitative and quantitative information about changes in the FA composition in plasma, RBCs, and FA-containing PC and PE in the retina.

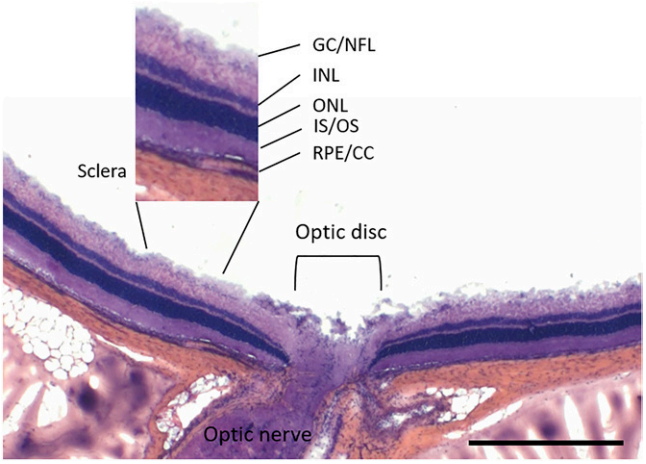

Fig. 5. H&E staining of ocular tissue section. GC/NFL, ganglion cell/nerve fiber layer; INL, inner nuclear layer; ONL, outer nuclear layer; IS/OS, inner segments/outer segments; RPE/CC, retinal pigment epithelium/choriocapillaris. Scale: 500 μm

The strength of our work is that LC n-3 EPA and DHA were provided in similar quantities either as PL or TG. Moreover, the formulations were balanced in FAs that could influence the incorporation of EPA or DHA into the retina, i.e., LA, ALA, and palmitic acid. Indeed, palmitic acid, as LA and ALA, is the substrate of FA desaturase 2 (FADS2), which mediates Δ6 desaturation of FA. Thus, palmitic acid, LA, and ALA can compete for the synthesis of desaturated metabolites and modify the efficiency of FADS2 to produce PUFAs (51). Despite limited variations in FAs, the five diets showed the same ratio of LA/ALA of 5 and the same amount of EPA+DHA provided either as PL or TG. The international society for the study of FAs and lipids (ISSFAL), international experts in nutrition and governmental agencies (French Agency for Food, Environmental and Occupational Health and Safety) recommend a LA/ALA ratio of 5 to fulfill the physiological requirements and prevent metabolic diseases, cardiovascular diseases, and AMD. In this study, we followed this recommendation for all diets. Meanwhile, Western countries are characterized by a dietary intake 20 times more rich in n-6 than in n-3 (52). The rationale for considering a fixed ratio between n-6 and n-3 FAs was based on the incorporation of DHA in the retina that depends on the LA/ALA ratio. Indeed, studies have shown that the decrease of LA intake benefits the n-3 incorporation into the retina in the rat (25), and to other tissues and human plasma (53, 54).

No clear evidence identifies whether PLs or TGs are the better dietary sources of n-3 PUFAs to improve their distribution into the retina (27, 50).

In plasma, our gas chromatographic analyses showed that EPA and DPA from the n-3 series were increased in rats fed with EPA-rich diets compared with control diet. Meanwhile, DHA was increased in DHA-rich diets compared with control, without significant differences between PL and TG forms. This result is consistent with the study in humans showing no difference in the increase of DHA levels in plasma when it was provided at the same dose, esterified in PL or TG (50). For EPA-rich diets, there was only a trend toward an increase in plasma DHA, confirming either the low conversion of EPA into DHA (22) or a rate of DHA utilization that equals DHA synthesis (55).

In RBCs, EPA was increased in all groups compared with control group, but particularly in EPA-rich diet groups. For all n-3 supplemented groups, there was an increase in n-3 DPA, the immediate DHA precursor, compared with the control group. DHA in RBCs was increased in groups fed with PL-EPA, PL-DHA, and TG-DHA diets, and to a lesser and insignificant extent in TG-EPA group. Similar results were obtained in the retina. This finding is consistent with previous data reporting that erythrocytes were better-circulating biomarkers of n-3 FAs in the retina than plasma (45) because they are less prone to dietary influence due to a life span of 120 days (56).

Interestingly, even if there was a similar increase in n-3 DPA in the retinas of TG-EPA and PL-EPA groups (160% and 162%, respectively, compared with control group),

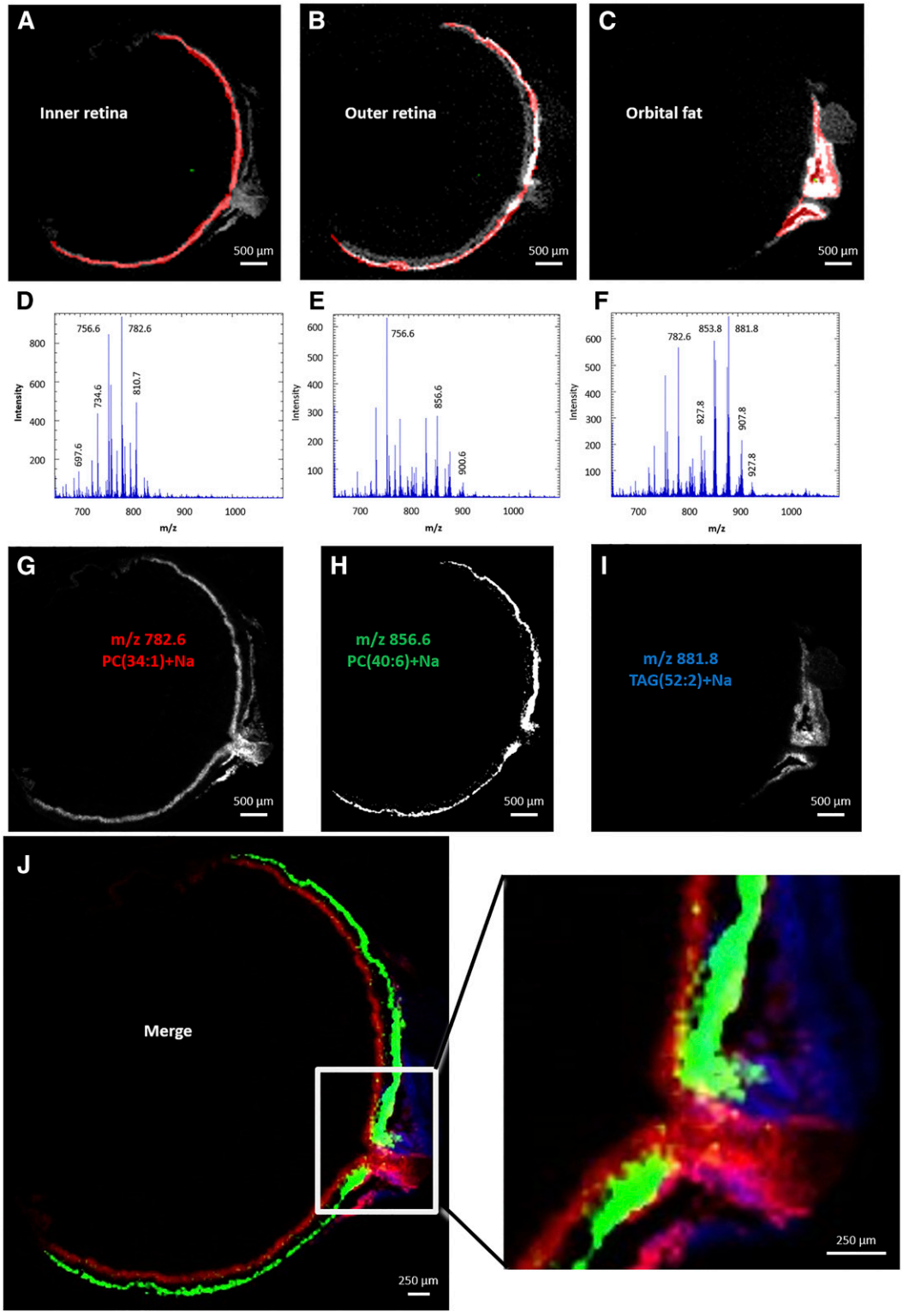

Fig. 6. Positive ion MALDI-IMS in rat ocular tissue. Regions of interest were selected as inner retina (A), outer retina (B), and orbital fat (C), corresponding to total positive ion MALDI mass spectra of inner retina (D), outer retina (E), and orbital fat (F). Extracted positive ion MALDI images of the $[M+Na]^+$ ions of PC34:1 (*m/z* 782.6 amu) (G), PC40:6 (*m/z* 856.6 amu) (H), and TG52:2 (*m/z* 881.8 amu) (I). J: Merged positive ion MALDI images of PC34:1 (red), PC40:6 (green), and TG52:2 (blue).

only a PL-EPA-rich diet triggered an increase of DHA in the retina (23% compared with control). Yet, both diets contained similar concentrations of DHA, meaning that the PL-EPA diet favored the incorporation of DHA in the retina compared with TG-EPA diet (as measured by the increase in DHA per increase in DPA). Moreover, RBCs in the PL-EPA group contained more DHA than the TG-EPA group. Besides, TG feeding may result in feedback

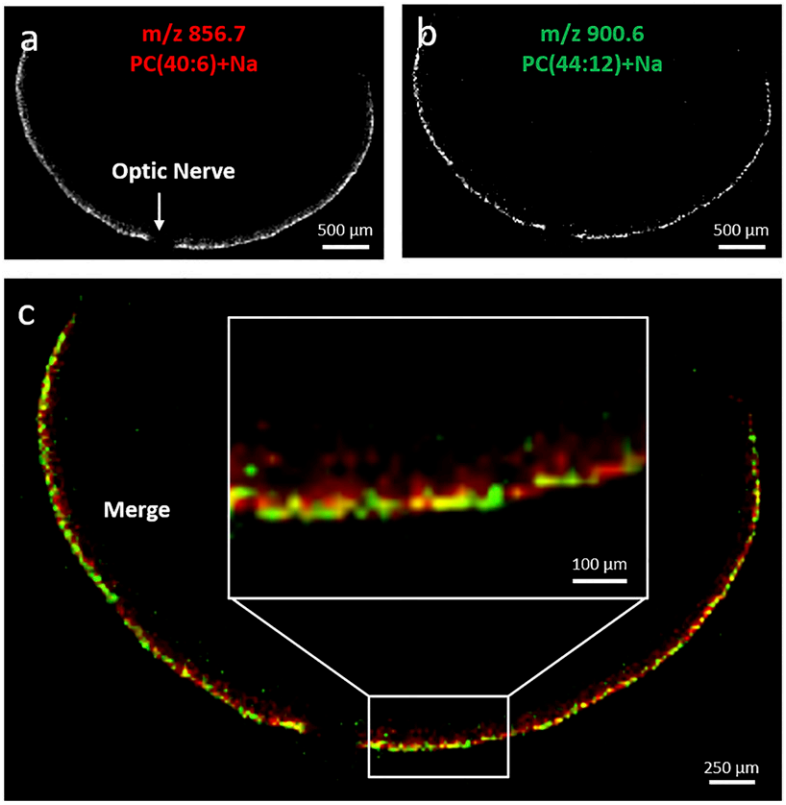

Fig. 7. Extracted positive ion MALDI images of the $[M+Na]^+$ of PC40:6 (*m/z* 856.7 amu) (A) and PC44:12 (*m/z* 900.6 amu) (B). Merged positive ion MALDI images of PC40:6 (red, total photoreceptor layer) and PC44:12 (green, photoreceptor outer segments) (C).

inhibition of n-3 DPA metabolism resulting in an accumulation of EPA and DPA in the retina. Our results are consistent with earlier findings showing that krill oil (PL-rich containing mostly EPA) favors β-oxidation and tissue deposition compared with fish oil (TG-rich diet) (57). Moreover, we may extrapolate a recent theory that is valid for the brain indicating that the absorption of EPA through the blood-brain barrier requires EPA as lysophosphatidylcholine, and to a lesser extent, as TG (58).

Concerning the DHA-rich diets, our results showed that the form under which DHA is esterified did not influence its bioavailability for the retina. Although the literature on this subject is controversial, it seems that most of the recent studies indicate that the incorporation of DHA in neural tissues is increased when DHA is provided as PLs compared with TGs (59, 60), especially in the presence of dietary DAGs and monoacylglycerols (MAGs) that facilitate micellar formation and thus enhance the LC n-3 FA uptake into enterocytes (61). However, the discrepancy with our results may be explained by the lower content in DAG and MAG in the PL-DHA diet than in the TG-DHA diet that may have mitigated the greater efficacy of PL-DHA diet to increase retinal DHA.

Our quantitative LC/MS analyses revealed an increase in DHA, especially DHA/DHA-containing PC (PC44:12) and PE (PE44:12), into the retina for all groups compared with control except TG-EPA. The effect that diet has on the EPA and DHA content is markedly different with little change observed in the retina. Large changes occurring in the RPE/choroid suggest that decisions concerning uptake and distribution of specific PCs to the retina are determined by the RPE/choroid.

Moreover, PL-EPA and TG-DHA diets increased VLC-PUFA-containing PC content into the retina. VLC-PUFA-containing glycerophospholipids are present at consistent levels in the retina compared with other tissues or organs (62) and give rise to lipid mediators called elovanoids, necessary for neuroprotective signaling for photoreceptor cell integrity (17, 63). ELOVL4 has been identified as a FA elongase protein that is involved in the synthesis of VLC-PUFAs (64). Its mutation leads to Stargardt disease, the most common hereditary form of macular dystrophy (65, 66). VLC-PUFAs are mainly esterified on PC species found in the retina in the sn-1 position of PCs that contain DHA in sn-2 position (67, 68).

It is of interest to note that dietary TG-EPA, as well as TG-DHA, increased VLC-PUFAs in the retina. This result is consistent with a previous study demonstrating that AA and EPA are preferred over DHA for the synthesis of VLC-PUFAs in the retina (69).

The lipid composition of the retina is remarkable because a molecular blueprint characterizes each particular layer. MALDI-IMS revealed the localization of DHA-containing PC into the photoreceptor layer of the retina. More precisely, PC44:12 (22:6/22:6) colocalized with PC40:6 (18:0/22:6), but the latter extends more into the inner part of the photoreceptor layer. Moreover, our study provides details on the localization of VLC-PUFAs relative to LC-PUFA-containing PC, and particularly PC44:12 (22:6/22:6) in the retina. Our MALDI images suggested that VLC-PUFAs would be localized in the external part of the retina similarly to PC44:12 (22:6/22:6). This localization seems to be crucial. Indeed, in Stargardt disease, mislocalization of the mutant protein may be at the origin of

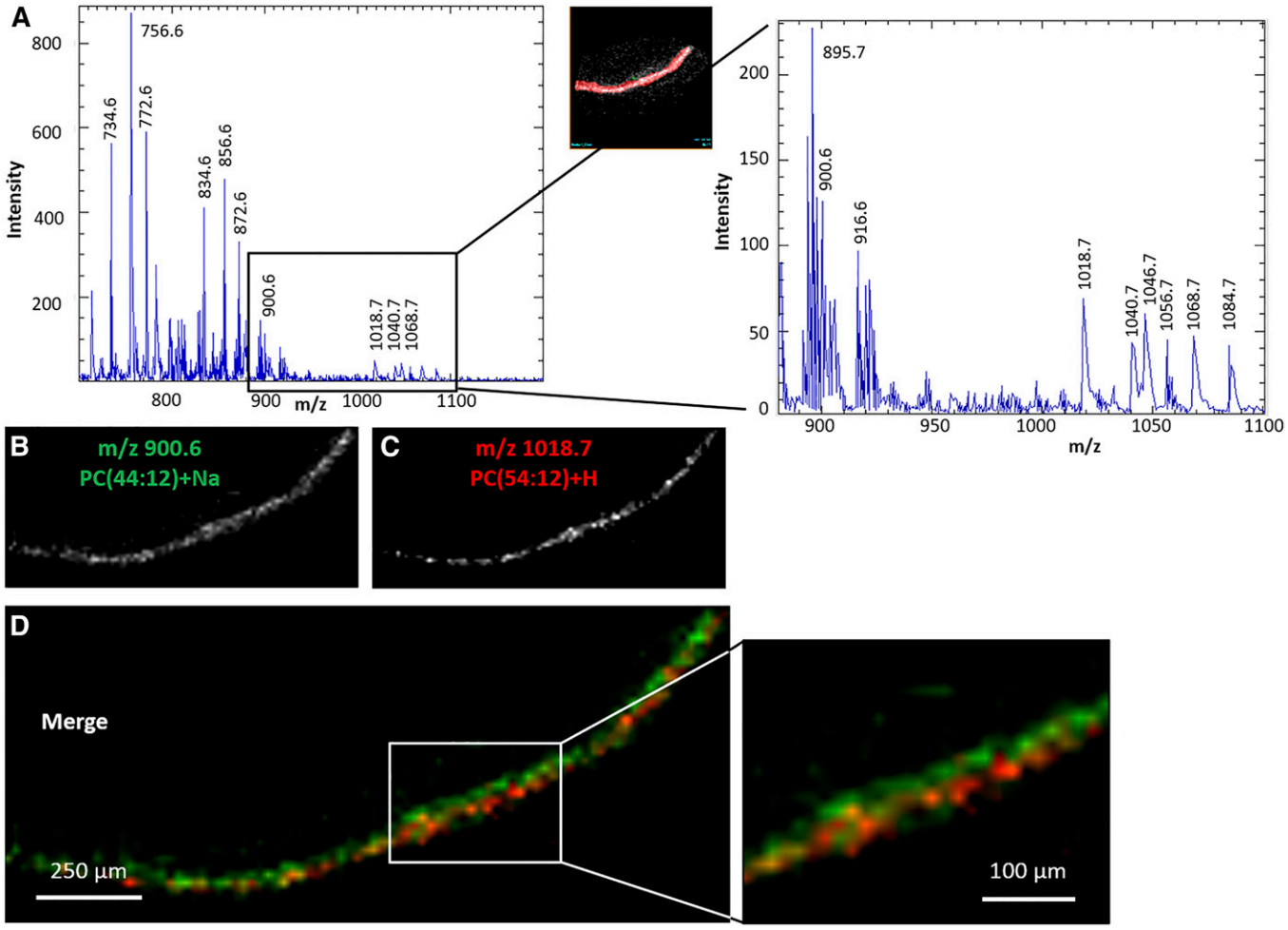

Fig. 8. Outer retina was selected as the region of interest, corresponding to total positive ion MALDI mass spectra (A). Extracted positive ion MALDI images of the [M+Na]+ of PC44:12 (*m/z* 900.6 amu, total photoreceptor layer) (B), and of the [M+H]+ of PC54:12 (*m/z* 1018.7 amu, photoreceptor outer segments) (C). D: Merged positive ion MALDI images of PC54:12 (red) and PC44:12 (green).

retinal degeneration, and the deletion of ELOVL4 leads to lipid and protein accumulation into the RPE (69).

VLC-PUFAs contribute to synaptic vesicle size, and thus synaptic transmission (70), and could be important for rod but not cone function (70, 71). Gaining details on VLC-PUFA location is essential for a better understanding of their function, because VLC-PUFAs are thought to be essential for the maintenance of the highly curved membrane disks of the photoreceptor outer segments (72). Rhodopsin is contained in outer segments, and the highest rhodopsin content is found in the retina of rats fed with diets containing DHA. Small manipulations of the dietary levels of AA and DHA are important determinants of FA composition of membrane lipid and visual pigment content (72).

MALDI-IMS confirmed results obtained with gas chromatography and LC-MS: enriched diets, particularly PL-EPA and TG-DHA, and to a lesser extent PL-DHA, favored the incorporation of DHA into the retina. Our results depicted in Fig. 9 indicate that this incorporation takes place in the photoreceptor layer, particularly in an area around the optic nerve. MALDI images do not provide quantitative information but highlight changes in localization and intensity of signal associated with PLs. Thus, there was an area near the optic nerve where the abundance of PC44:12 (22:6/22:6) was extremely high in all supplemented diet groups compared with the control group. This area was previously described in a study of Cortina as the area that is the most sensitive to oxidative stress induced by bright light treatment in rats (73). In this study, light-induced oxidative stress compromised photoreceptor integrity, particularly in an area next to the optic nerve, in the superior and nasal quadrant, suggesting that photoreceptors are most sensitive in this area. This particular response could mean that, because the outer segments contain a greater number of discs and, thus, higher PUFA levels, a greater sensitivity to oxidative stress may occur. Because this area contains more discs, it would be more prone to incorporate DHA from dietary intake than other regions. As well, the high incorporation of the DHA and the other PUFAs in the retina may result in more plastic membranes, allowing more efficient phototransduction and synaptic function (10–12, 74). Further experiments should be necessary to explore whether the uptake capacity or the VLC-PUFA synthesis is increased in that zone in these conditions.

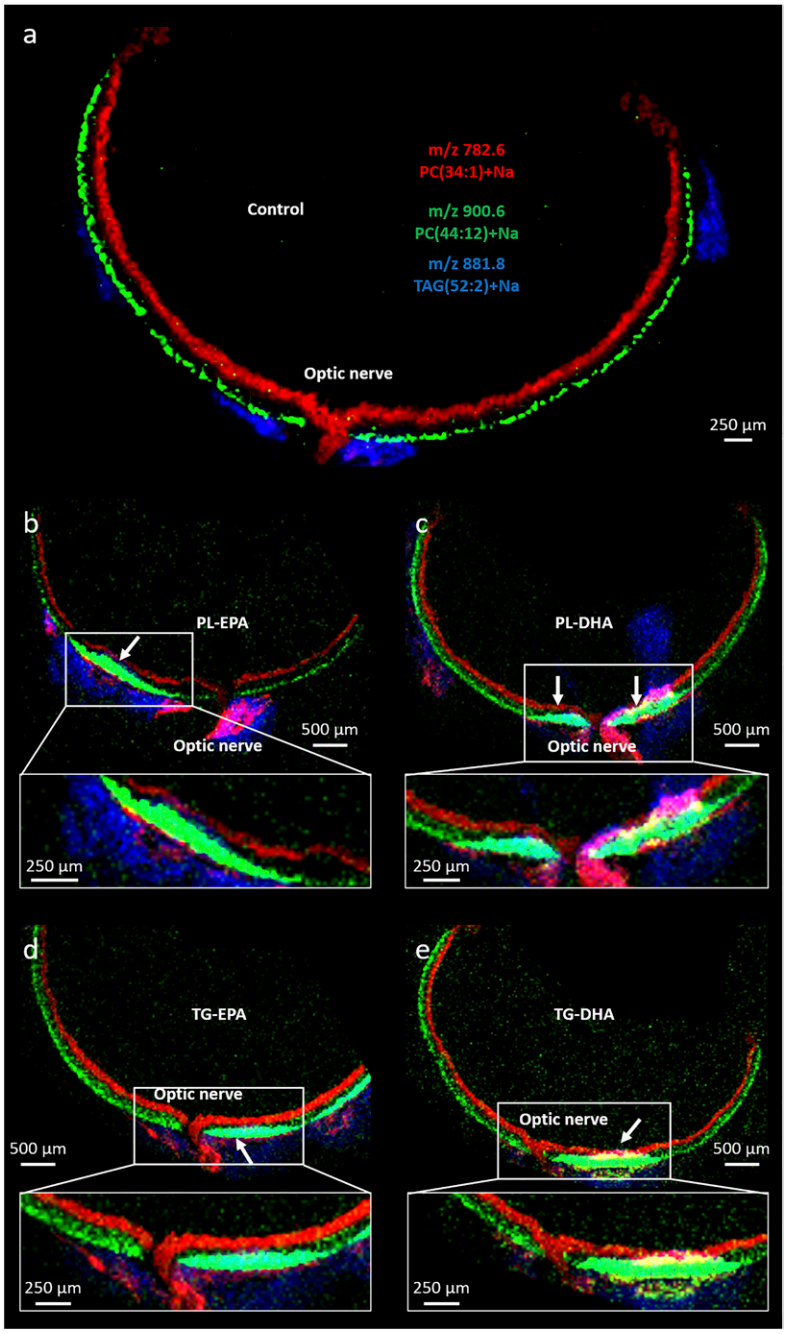

Fig. 9. PC(DHA/DHA) intensity is increased next to the optic nerve in n-3 supplemented groups (arrows). Merged positive ion MALDI images of PC34:1 (red, inner retina), PC44:12 (green, photoreceptor outer segments) and TG52:2 (blue, orbital fat) for the group control (a), PL-EPA (b), PL-DHA (c), TG-EPA (d), TG-DHA (e). PC44:12).

To our knowledge, for the first time, our study provides quantitative data on VLC-PUFA changes following different n-3 rich diets. Our data provides a high level of qualitative and quantitative details on molecular species and FA in the plasma, RBCs, and retina. The main findings in this study were that both EPA and DHA enhanced DHA increase in the retina and that FAs provided by diet can trigger changes in spatial lipid organization of the retina, mainly RPE/choroid. Especially, EPA esterified on PLs is as efficient as DHA-rich diets to increase DHA level in retina, as well as VLC-PUFAs. Further research is needed to better understand the mechanisms regulating how FAs containing PLs or TGs travel from oral uptake through the digestive tract to the retina and RPE.

Data availability

The data that support the findings of this study are available from the corresponding author and online (https://data.inrae.fr).

Acknowledgments

The authors would like to thank the CSGA animal facility for excellent animal care and AkerBiomarine and Novastell for having supplied us with raw materials.

Author contributions

E.V., B.J., W.C.G., S.K., O.B., N.A., L.B., and N.G.B. conceptualization; E.V., B.J., W.C.G., S.K., O.B., N.A., L.B., and N.G.B. design; E.V., B.J., W.C.G., M-A.M., L.M., S.G., S.K., and S.C. data acquisition and/or analyses; E.V., B.J., W.C.G.,

S.K., S.C., O.B., N.A., L.B., and N.G.B. data interpretation; E.V., B.J., W.C.G., S.K., S.C., L.B., and N.G.B. writing. All authors reviewed the final version of the manuscript.

Funding and other information

This work was supported by the Regional Council of Burgundy France, FEDER (European Funding for Regional Economical Development), Association Nationale Recherche Technologie, Fondation de France/Fondation de l'Oeil. Grant ANR-11-LABEX-0021 was provided by the French National Research Agency (ANR). Additional support was provided by National Eye Institute Grant EY005121 and the Eye Ear Nose Throat (EENT) Foundation of New Orleans to N.B.Z. E.V. is a PhD fellow from Horus Pharma Laboratories. The content is solely the responsibility of the authors and does not necessarily represent the official views of the National Institutes of Health.

Conflict of interest

The authors declare that they have no conflicts of interest with the contents of this article.

Abbreviations

ACN, acetonitrile; ALA, α-linolenic acid; AMD, age-related macular degeneration; DHB, 2,5-dihydroxybenzoic acid; DPA, docosapentaenoic acid; ELOVL, elongation of very long chain fatty-acids; HILIC, hydrophilic interaction LC; IMS, imaging MS; LA, linoleic acid; LC-PUFA, long chain PUFA; MAG, monoacylglycerol; PL, phospholipid; RBC, red blood cell; RPE, retinal pigment epithelium; VLC-PUFA, very long chain PUFA.

Manuscript received July 31, 2020, and in revised form October 26, 2020. Published, JLR Papers in Press, October 30, 2020, DOI 10.1194/jlr.RA120001057.

REFERENCES

1. Flaxman, S. R., R. R. A. Bourne, S. Resnikoff, P. Ackland, T. Braithwaite, M. V. Cicinelli, A. Das, J. B. Jonas, J. Keeffe, J. H. Kempen, et al. 2017. Global causes of blindness and distance vision impairment 1990–2020: a systematic review and meta-analysis. *Lancet Glob. Health.* **5:** e1221–e1234.
2. Klaver, C. C., R. C. Wolfs, J. R. Vingerling, A. Hofman, and P. T. de Jong. 1998. Age-specific prevalence and causes of blindness and visual impairment in an older population: the Rotterdam Study. *Arch. Ophthalmol.* **116:** 653–658.
3. Querques, G., R. Forte, and E. H. Souied. 2011. Retina and omega-3. *J. Nutr. Metab.* **2011:** 748361.
4. Kishan, A. U., B. S. Modjtahedi, E. N. Martins, S. P. Modjtahedi, and L. S. Morse. 2011. Lipids and age-related macular degeneration. *Surv. Ophthalmol.* **56:** 195–213.
5. Liu, A., J. Chang, Y. Lin, Z. Shen, and P. S. Bernstein. 2010. Long-chain and very long-chain polyunsaturated fatty acids in ocular aging and age-related macular degeneration. *J. Lipid Res.* **51:** 3217–3229.
6. Fliesler, S. J., and R. E. Anderson. 1983. Chemistry and metabolism of lipids in the vertebrate retina. *Prog. Lipid Res.* **22:** 79–131.
7. Bretillon, L., G. Thuret, S. Gregoire, N. Acar, C. Joffre, A. M. Bron, P. Gain, and C. P. Creuzot-Garcher. 2008. Lipid and fatty acid profile of the retina, retinal pigment epithelium/choroid, and the lacrimal gland, and associations with adipose tissue fatty acids in human subjects. *Exp. Eye Res.* **87:** 521–528.
8. Brown, M. F. 1994. Modulation of rhodopsin function by properties of the membrane bilayer. *Chem. Phys. Lipids.* **73:** 159–180.
9. Gawrisch, K., O. Soubias, and M. Mihailescu. 2008. Insights from biophysical studies on the role of polyunsaturated fatty acids for function of G-protein coupled membrane receptors. *Prostaglandins Leukot. Essent. Fatty Acids.* **79:** 131–134.
10. Litman, B. J., S. L. Niu, A. Polozova, and D. C. Mitchell. 2001. The role of docosahexaenoic acid containing phospholipids in modulating G protein-coupled signaling pathways: visual transduction. *J. Mol. Neurosci.* **16:** 237–242, discussion 79–84.
11. Mitchell, D. C., S. L. Niu, and B. J. Litman. 2001. Optimization of receptor-G protein coupling by bilayer lipid composition I: kinetics of rhodopsin-transducin binding. *J. Biol. Chem.* **276:** 42801–42806.
12. Niu, S. L., D. C. Mitchell, and B. J. Litman. 2001. Optimization of receptor-G protein coupling by bilayer lipid composition II: formation of metarhodopsin II-transducin complex. *J. Biol. Chem.* **276:** 42807–42811.
13. Suh, M., and M. T. Clandinin. 2005. 20:5n-3 but not 22:6n-3 is a preferred substrate for synthesis of n-3 very-long- chain fatty acids (C24–C36) in retina. *Curr. Eye Res.* **30:** 959–968.
14. Yu, M., A. Benham, S. Logan, R. S. Brush, M. N. Mandal, R. E. Anderson, and M-P. Agbaga. 2012. ELOVL4 protein preferentially elongates 20:5n3 to very long chain PUFAs over 20:4n6 and 22:6n3. *J. Lipid Res.* **53:** 494–504.
15. Bannenberg, G., and C. N. Serhan. 2010. Specialized pro-resolving lipid mediators in the inflammatory response: An update. *Biochim. Biophys. Acta.* **1801:** 1260–1273.
16. Bazan, N. G. 2005. Neuroprotectin D1 (NPD1): a DHA-derived mediator that protects brain and retina against cell injury-induced oxidative stress. *Brain Pathol.* **15:** 159–166.
17. Jun, B., P. K. Mukherjee, A. Asatryan, M. A. Kautzmann, J. Heap, W. C. Gordon, S. Bhattcharjee, R. Yang, N. A. Petasis, and N. G. Bazan. 2017. Elovanoids are novel cell-specific lipid mediators necessary for neuroprotective signaling for photoreceptor cell integrity. *Sci. Rep.* **7:** 5279.
18. Bazan, N. G. 2018. Docosanoids and elovanoids from omega-3 fatty acids are pro-homeostatic modulators of inflammatory responses, cell damage and neuroprotection. *Mol. Aspects Med.* **64:** 18–33.
19. Burdge, G. C., and P. C. Calder. 2005. Conversion of alpha-linolenic acid to longer-chain polyunsaturated fatty acids in human adults. *Reprod. Nutr. Dev.* **45:** 581–597.
20. Burdge, G. C., and S. A. Wootton. 2002. Conversion of alpha-linolenic acid to eicosapentaenoic, docosapentaenoic and docosahexaenoic acids in young women. *Br. J. Nutr.* **88:** 411–420.
21. Pawlosky, R. J., J. R. Hibbeln, J. A. Novotny, and N. Salem, Jr. 2001. Physiological compartmental analysis of alpha-linolenic acid metabolism in adult humans. *J. Lipid Res.* **42:** 1257–1265.
22. Plourde, M., and S. C. Cunnane. 2007. Extremely limited synthesis of long chain polyunsaturates in adults: implications for their dietary essentiality and use as supplements. *Appl. Physiol. Nutr. Metab.* **32:** 619–634.
23. Harris, W. S. 2007. International recommendations for consumption of long-chain omega-3 fatty acids. *J. Cardiovasc. Med. (Hagerstown).* **8 (Suppl. 1):** S50–S52.
24. Schuchardt, J. P., and A. Hahn. 2013. Bioavailability of long-chain omega-3 fatty acids. *Prostaglandins Leukot. Essent. Fatty Acids.* **89:** 1–8.
25. Simon, E., B. Bardet, S. Gregoire, N. Acar, A. M. Bron, C. P. Creuzot-Garcher, and L. Bretillon. 2011. Decreasing dietary linoleic acid promotes long chain omega-3 fatty acid incorporation into rat retina and modifies gene expression. *Exp. Eye Res.* **93:** 628–635.
26. SanGiovanni, J. P., E. Y. Chew, T. E. Clemons, M. D. Davis, F. L. Ferris III, G. R. Gensler, N. Kurinij, A. S. Lindblad, R. C. Milton, J. M. Seddon, et al. 2007. The relationship of dietary lipid intake and age-related macular degeneration in a case-control study: AREDS Report No. 20. *Arch. Ophthalmol.* **125:** 671–679.
27. Salem, N., Jr., and C. N. Kuratko. 2014. A reexamination of krill oil bioavailability studies. *Lipids Health Dis.* **13:** 137.
28. Ackman, R. G. 1981. Flame ionization detection applied to thin-layer chromatography on coated quartz rods. *Methods Enzymol.* **72:** 205–252.
29. Folch, J., M. Lees, and G. H. Sloane Stanley. 1957. A simple method for the isolation and purification of total lipides from animal tissues. *J. Biol. Chem.* **226:** 497–509.
30. Moilanen, T., and T. Nikkari. 1981. The effect of storage on the fatty acid composition of human serum. *Clin. Chim. Acta.* **114:** 111–116.
31. Morrison, W. R., and L. M. Smith. 1964. Preparation of fatty acid methyl esters and dimethylacetals from lipids with boron fluoride–methanol. *J. Lipid Res.* **5:** 600–608.
32. Bartlett, E. M., and D. H. Lewis. 1970. Spectrophotometric determination of phosphate esters in the presence and absence of orthophosphate. *Anal. Biochem.* **36:** 159–167.
33. Le Bon, A. M., N. Depretre, E. Sibille, S. Cabaret, S. Gregoire, V. Soubeyre, E. Masson, N. Acar, L. Bretillon, X. Grosmaitre, et al. 2018.

Comprehensive study of rodent olfactory tissue lipid composition. *Prostaglandins Leukot. Essent. Fatty Acids.* **131:** 32–43.
34. Kautzmann, M. A. I., W. C. Gordon, B. Jun, K. V. Do, B. J. Matherne, Z. Fang, and N. G. Bazan. 2020. Membrane-type frizzled-related protein regulates lipidome and transcription for photoreceptor function. *FASEB J.* **34:** 912–929.
35. Hankin, J. A., R. M. Barkley, and R. C. Murphy. 2007. Sublimation as a method of matrix application for mass spectrometric imaging. *J. Am. Soc. Mass Spectrom.* **18:** 1646–1652.
36. Zemski Berry, K. A., W. C. Gordon, R. C. Murphy, and N. G. Bazan. 2014. Spatial organization of lipids in the human retina and optic nerve by MALDI imaging mass spectrometry. *J. Lipid Res.* **55:** 504–515.
37. Ko, C. W., J. Qu, D. D. Black, and P. Tso. 2020. Regulation of intestinal lipid metabolism: current concepts and relevance to disease. *Nat. Rev. Gastroenterol. Hepatol.* **17:** 169–183.
38. D'Aquila, T., Y. H. Hung, A. Carreiro, and K. K. Buhman. 2016. Recent discoveries on absorption of dietary fat: Presence, synthesis, and metabolism of cytoplasmic lipid droplets within enterocytes. *Biochim. Biophys. Acta.* **1861(8 Pt A):** 730–747.
39. Kararli, T. T. 1995. Comparison of the gastrointestinal anatomy, physiology, and biochemistry of humans and commonly used laboratory animals. *Biopharm. Drug Dispos.* **16:** 351–380.
40. Hryn, V. H., Y. P. Kostylenko, V. P. Bilash, and O. B. Ryabushko. 2019. Microscopic structure of albino rats' small intestine. *Wiad. Lek.* **72:** 733–738.
41. SanGiovanni, J. P., and E. Y. Chew. 2005. The role of omega-3 long-chain polyunsaturated fatty acids in health and disease of the retina. *Prog. Retin. Eye Res.* **24:** 87–138.
42. Agbaga, M. P., M. N. Mandal, and R. E. Anderson. 2010. Retinal very long-chain PUFAs: new insights from studies on ELOVL4 protein. *J. Lipid Res.* **51:** 1624–1642.
43. Cho, E., S. Hung, W. C. Willett, D. Spiegelman, E. B. Rimm, J. M. Seddon, G. A. Colditz, and S. E. Hankinson. 2001. Prospective study of dietary fat and the risk of age-related macular degeneration. *Am. J. Clin. Nutr.* **73:** 209–218.
44. Seddon, J. M., B. Rosner, R. D. Sperduto, L. Yannuzzi, J. A. Haller, N. P. Blair, and W. Willett. 2001. Dietary fat and risk for advanced age-related macular degeneration. *Arch. Ophthalmol.* **119:** 1191–1199.
45. Acar, N., O. Berdeaux, S. Gregoire, S. Cabaret, L. Martine, P. Gain, G. Thuret, C. P. Creuzot-Garcher, A. M. Bron, and L. Bretillon. 2012. Lipid composition of the human eye: are red blood cells a good mirror of retinal and optic nerve fatty acids? *PLoS One.* **7:** e35102.
46. Gorusupudi, A., A. Liu, G. S. Hageman, and P. S. Bernstein. 2016. Associations of human retinal very long-chain polyunsaturated fatty acids with dietary lipid biomarkers. *J. Lipid Res.* **57:** 499–508.
47. Ramprasath, V. R., I. Eyal, S. Zchut, and P. J. Jones. 2013. Enhanced increase of omega-3 index in healthy individuals with response to 4-week n-3 fatty acid supplementation from krill oil versus fish oil. *Lipids Health Dis.* **12:** 178.
48. Schuchardt, J. P., I. Schneider, H. Meyer, J. Neubronner, C. von Schacky, and A. Hahn. 2011. Incorporation of EPA and DHA into plasma phospholipids in response to different omega-3 fatty acid formulations–a comparative bioavailability study of fish oil vs. krill oil. *Lipids Health Dis.* **10:** 145.
49. Ulven, S. M., B. Kirkhus, A. Lamglait, S. Basu, E. Elind, T. Haider, K. Berge, H. Vik, and J. I. Pederson. 2011. Metabolic effects of krill oil are essentially similar to those of fish oil but at lower dose of EPA and DHA, in healthy volunteers. *Lipids.* **46:** 37–46.
50. Yurko-Mauro, K., J. Kralovec, E. Bailey-Hall, V. Smeberg, J. G. Stark, and N. Salem, Jr. 2015. Similar eicosapentaenoic acid and docosahexaenoic acid plasma levels achieved with fish oil or krill oil in a randomized double-blind four-week bioavailability study. *Lipids Health Dis.* **14:** 99.
51. Park, H. G., K. S. D. Kothapalli, W. J. Park, C. DeAllie, L. Liu, A. Liang, P. Lawrence, and J. T. Brenna. 2016. Palmitic acid (16:0) competes with omega-6 linoleic and omega-3 a-linolenic acids for FADS2 mediated Delta6-desaturation. *Biochim. Biophys. Acta.* **1861:** 91–97.
52. Simopoulos, A. P. 2002. The importance of the ratio of omega-6/omega-3 essential fatty acids. *Biomed. Pharmacother.* **56:** 365–379.
53. Blanchard, H., F. Pedrono, N. Boulier-Monthean, D. Catheline, V. Rioux, and P. Legrand. 2013. Comparative effects of well-balanced diets enriched in alpha-linolenic or linoleic acids on LC-PUFA metabolism in rat tissues. *Prostaglandins Leukot. Essent. Fatty Acids.* **88:** 383–389.
54. Taha, A. Y., Y. Cheon, K. F. Faurot, B. Macintosh, S. F. Majchrzak-Hong, J. D. Mann, J. R. Hibbeln, A. Ringel, and C. E. Ramsden. 2014. Dietary omega-6 fatty acid lowering increases bioavailability of omega-3 polyunsaturated fatty acids in human plasma lipid pools. *Prostaglandins Leukot. Essent. Fatty Acids.* **90:** 151–157.
55. Metherel, A. H., and R. P. Bazinet. 2019. Updates to the n-3 polyunsaturated fatty acid biosynthesis pathway: DHA synthesis rates, tetracosahexaenoic acid and (minimal) retroconversion. *Prog. Lipid Res.* **76:** 101008.
56. Ebaugh, F. G., Jr., C. P. Emerson, and J. F. Ross. 1953. The use of radioactive chromium 51 as an erythrocyte tagging agent for the determination or red cell survival in vivo. *J. Clin. Invest.* **32:** 1260–1276.
57. Ghasemifard, S., K. Hermon, G. M. Turchini, and A. J. Sinclair. 2015. Metabolic fate (absorption, beta-oxidation and deposition) of long-chain n-3 fatty acids is affected by sex and by the oil source (krill oil or fish oil) in the rat. *Br. J. Nutr.* **114:** 684–692.
58. Yalagala, P. C. R., D. Sugasini, S. Dasarathi, K. Pahan, and P. V. Subbaiah. 2019. Dietary lysophosphatidylcholine-EPA enriches both EPA and DHA in the brain: potential treatment for depression. *J. Lipid Res.* **60:** 566–578.
59. Chouinard-Watkins, R., R. J. S. Lacombe, A. H. Metherel, M. Masoodi, and R. P. Bazinet. 2019. DHA esterified to phosphatidylserine or phosphatidylcholine is more efficient at targeting the brain than DHA esterified to triacylglycerol. *Mol. Nutr. Food Res.* **63:** e1801224.
60. Zahid, A., and M. Reicks. 2018. Gain-framed messages were related to higher motivation scores for sugar-sweetened beverage parenting practices than loss-framed messages. *Nutrients.* **10:** 625.
61. Dyerberg, J., P. Madsen, J. M. Moller, I. Aardestrup, and E. B. Schmidt. 2010. Bioavailability of marine n-3 fatty acid formulations. *Prostaglandins Leukot. Essent. Fatty Acids.* **83:** 137–141.
62. Aveldaño, M. I. 1988. Phospholipid species containing long and very long polyenoic fatty acids remain with rhodopsin after hexane extraction of photoreceptor membranes. *Biochemistry.* **27:** 1229–1239.
63. Do, K. V., M. I. Kautzmann, B. Jun, W. C. Gordon, R. Nshimiyimana, R. Yang, N. A. Petasis, and N. G. Bazan. 2019. Elovanoids counteract oligomeric beta-amyloid-induced gene expression and protect photoreceptors. *Proc. Natl. Acad. Sci. USA.* **116:** 24317–24325.
64. Agbaga, M. P., R. S. Brush, M. N. Mandal, K. Henry, M. H. Elliott, and R. E. Anderson. 2008. Role of Stargardt-3 macular dystrophy protein (ELOVL4) in the biosynthesis of very long chain fatty acids. *Proc. Natl. Acad. Sci. USA.* **105:** 12843–12848.
65. Zhang, K., M. Kniazeva, M. Han, W. Li, Z. Yu, Z. Yang, Y. Li, M. L. Metzker, R. Allikmets, D. J. Zack. 2001. A 5-bp deletion in ELOVL4 is associated with two related forms of autosomal dominant macular dystrophy. *Nat. Genet.* **27:** 89–93.
66. Hopiavuori, B. R., R. E. Anderson, and M. P. Agbaga. 2019. ELOVL4: very long-chain fatty acids serve an eclectic role in mammalian health and function. *Prog. Retin. Eye Res.* **69:** 137–158.
67. Aveldaño, M. I., and H. Sprecher. 1987. Very long chain (C24 to C36) polyenoic fatty acids of the n-3 and n-6 series in dipolyunsaturated phosphatidylcholines from bovine retina. *J. Biol. Chem.* **262:** 1180–1186.
68. Harkewicz, R., H. Du, Z. Tong, H. Alkuraya, M. Bedell, W. Sun, X. Wang, Y-H. Hsu, J. Esteve-Rudd, G. Hughes, et al. 2012. Essential role of ELOVL4 protein in very long chain fatty acid synthesis and retinal function. *J. Biol. Chem.* **287:** 11469–11480.
69. Agbaga, M. P., S. Logan, R. S. Brush, and R. E. Anderson. 2014. Biosynthesis of very long-chain polyunsaturated fatty acids in hepatocytes expressing ELOVL4. *Adv. Exp. Med. Biol.* **801:** 631–636.
70. Bennett, L. D., B. R. Hopiavuori, R. S. Brush, M. Chan, M. J. Van Hook, W. B. Thoreson, and R. E. Anderson. 2014. Examination of VLC-PUFA-deficient photoreceptor terminals. *Invest. Ophthalmol. Vis. Sci.* **55:** 4063–4072.
71. Schori, C., M. P. Agbaga, R. S. Brush, R. Ayyagari, C. Grimm, and M. Samardzija. 2018. Elovl4 5-bp deletion does not accelerate cone photoreceptor degeneration in an all-cone mouse. *PLoS One.* **13:** e0190514.
72. Suh, M., A. A. Wierzbicki, E. L. Lien, and M. T. Clandinin. 2000. Dietary 20:4n-6 and 22:6n-3 modulates the profile of long- and very-long-chain fatty acids, rhodopsin content, and kinetics in developing photoreceptor cells. *Pediatr. Res.* **48:** 524–530.
73. Cortina, M. S., W. C. Gordon, W. J. Lukiw, and N. G. Bazan. 2005. Oxidative stress-induced retinal damage up-regulates DNA polymerase gamma and 8-oxoguanine-DNA-glycosylase in photoreceptor synaptic mitochondria. *Exp. Eye Res.* **81:** 742–750.
74. Mitchell, D. C., S. L. Niu, and B. J. Litman. 2003. Enhancement of G protein-coupled signaling by DHA phospholipids. *Lipids.* **38:** 437–443.